Two-soliton and three-soliton molecules in optical fibers

P. Rohrmann, A. Hause, and F. Mitschke*
Institut für Physik, Universität Rostock, 18051 Rostock, Germany
(Received 12 February 2013; published 25 April 2013)

An experimental study of bound states of two solitons and of three solitons in dispersion-managed fibers is presented. The existence regime and stability of such soliton molecules is investigated. With a programmable pulse shaper we can flexibly shape launch signals; received signals are detected in amplitude and phase, and in relative position and velocity. An equilibrium separation is demonstrated for both two-soliton and three-soliton soliton molecules. It is also shown that stable molecules are possible only with antiphase pulses. Both types of soliton molecule are viable for transmission in the same fiber, at the same wavelength. Together with single solitons this opens the possibility of quaternary data transmission in a soliton-based format.

DOI: 10.1103/PhysRevA.87.043834 PACS number(s): 42.81.Dp, 42.65.Re, 42.79.Sz

I. INTRODUCTION

Today's telephone and internet traffic is accommodated by massive streams of short light pulses passing through optical fibers. To keep up with the ever-increasing demand by data-hungry applications, the data-carrying capacity of fibers must be pushed up further. A useful benchmark is Shannon's theorem [1] which, however, was written with amplitude modulation of an rf carrier in mind. Optical fibers provide the additional possibilities of coherent (phase) detection and of polarization multiplexing to improve the capacity over Shannon's discussion. On the other hand, optical fiber is a nonlinear medium, and mixing products between signals are a detriment. All told, the improvement over Shannon's result is not dramatic [2,3]. As was recently pointed out, however, nonlinearity may also be put to an advantage so that an improvement over the Shannon limit becomes possible [4].

According to Shannon's theorem, the capacity is given by the available bandwidth and by a factor depending on the coding in the presence of noise. The bandwidth in optical fibers can be estimated as 30–50 THz depending on how much loss one deems acceptable; it is not anticipated that this figure can be substantially improved by any available means. The other factor is the binary logarithm of either the signal-to-noise ratio (in an analog system) or the number of symbols distinguished in the transmission (which is always less than the former). In the particularly simple case of binary coding, which is used in the bulk of all transmission systems in operation today, there are just two symbols, typically the absence of light (logical *Zero*) within a clock period, or a single pulse (logical *One*). The clock period is often 25 ps, corresponding to a 40 Gbits/s transmission rate. Without invoking further refinements, in such a system the numerical value of the capacity equals that of the bandwidth, i.e., 30–50 Tbits/s.

No single data source can ever provide such an enormous data rate. In today's transmission systems one employs wavelength division multiplexing of many data sources where multiple channels at different optical frequencies are used simultaneously. This technique allows one to come close to the Shannon limit for binary coding using a multitude of manageable 40 Gbits/s channels. However, the demand grows so rapidly that one is now faced with a "capacity crunch" [5]. Economic considerations favor the continued use of existing (legacy) fibers. But then the only option for further improvement is to find coding schemes which go beyond the binary format.

Current suggestions include the use of pulses with different polarization, phase, and peak power as different symbols. Two orthogonal states of polarization provide an extra bit of information per clock period, provided that the cross talk between the orthogonal states is kept in check. The arrangement of phase and amplitude values is often displayed as the "configuration space," a complex plane in which each symbol is represented by a point. If all symbols are on a circle around the origin, they all have the same power so that a minimum of nonlinear distortion is expected. For example, quaternary phase-shift keying successfully provides one extra bit per clock period. If more states are added (as in quadrature amplitude modulation, etc.), however, one has to keep in mind that each symbol is affected by noise; just as in Shannon's case they must not get too close to each other in configuration space. Typically the power is kept quite low to avoid nonlinear effects, or some complex correction is employed—and often a combination of both. Highly respectable results have been obtained along these lines by using sophisticated coding schemes combined with complex error-compensation techniques (for a recent review see [6]), and some of these methods are in commercial use already. But ultimately the available number of symbols is limited to the available configuration-space area, divided by the "noise ball" assigned to each symbol. When one approaches this limit, basically one returns to an analog system. This is peculiar as it was precisely the robustness of binary systems that led to the abandonment of linear systems many years ago.

The central idea of Ref. [4] is that as the noise builds up gradually during transmission, nonlinearity can be employed to repeatedly collapse each noise ball to its center point; then symbols can be packed more densely in configuration space so that the capacity is increased. In this way, nonlinearity can be used to exceed the Shannon limit.

The following presentation is organized as follows: After outlining the soliton molecule concept in general in Sec. II, we introduce the experimental setup for the multipulse generation, pulse propagation, and measurement in Sec. III. In Sec. IV we present experimental results concerning the two-soliton

*fedor.mitschke@uni-rostock.de; URL:www.physik.uni-rostock.de/optik.

molecule. In this detailed study the existence regimes and relative phase dependencies of these soliton pairs are determined. Section V is similar to Sec. IV but for the three-soliton case. Section VI deals with the possibility of a simultaneous transmission of four soliton-based coding symbols in the same transmission line; this is followed by some conclusions in Sec. VII.

II. THE SOLITON MOLECULE CONCEPT

Here we suggest an alternative approach in which also nonlinearity is put to good use. In our proposal the fiber's nonlinearity is used to form soliton molecules; a brief account was already given in Ref. [7]. Soliton molecules are based on *solitons*, a stable kind of light pulse in fibers that was predicted in 1973 [8] and first demonstrated in 1980 [9]. They are stable solutions of the underlying nonlinear propagation equation, the nonlinear Schrödinger equation (NLSE) [10,11], and therefore they have been considered by many to be the natural bits for optical telecommunication. Solitons rely on a stable balance between the nonlinearity-induced phase modulation and linear dispersive effects. They are robust in the presence of perturbations: the fact that they are stable solutions of the wave equation implies that perturbations can heal out to some degree. Around the year 2000 solitons began to be used in a few commercial systems, but in most recent research they were discounted as supposedly useful for binary coding only. This may have been premature.

For a discussion of possible coding formats we first need to point out that the preferred type of fibers is now the so-called dispersion-managed (DM) fiber. DM fibers consist of fiber segments with alternating positive and negative group-velocity dispersion coefficients. The combined length of one positive and one negative dispersion segment is called the dispersion period. Typically, DM fiber lines begin and end with a half segment of one of the fibers. The advantage of DM fibers over conventional constant-dispersion fibers is that they simultaneously have high local and small path-average dispersion. The former is beneficial for suppression of four-wave-mixing effects whereas the latter helps keeping overall dispersive effects low (in linear systems; in soliton systems it keeps the power requirements low). Several groups have shown almost simultaneously that in DM fibers solitonlike pulses exist [12–16]; they are called DM solitons. Their shape is different from that of standard solitons (closer to a Gaussian rather than a hyperbolic secant [17,18]), and all pulse parameters "breathe" in the dispersion period. As they periodically return to their initial values, the pulse shape is stable *in the stroboscopic sense* (i.e., when sampled once per dispersion period).

Interaction forces between copropagating pulses are mediated by the Kerr effect in the fiber. It has been known for a long time that, depending on the relative phase of the solitons, there can be attraction or repulsion [19,20]. In constant-dispersion fibers two pulses of the same energy and velocity can, depending on their relative phase φ, either attract ($\varphi = 0$) or repel each other ($\varphi = \pi$), or exchange energy ($\varphi \neq 0,\pi$). Equal-energy soliton pairs with constant temporal separation do not exist in constant-dispersion fibers. In DM fibers the situation is much more complex: there is not even a fixed phase relationship as the width and chirp breathe. It has turned out, however, that a stable bound state of DM solitons exists. We have experimentally demonstrated the existence of stable antiphase soliton pairs [21]; this had also been noted before in theoretical work [22–25] and was recently also pursued in Refs. [26,27]. The pairs have a favored temporal separation which is characterized by a stable equilibrium of attracting and repelling forces. This is reminiscent of the equilibrium spatial separation of two nuclei in a diatomic molecule; we therefore called this structure a "soliton molecule." The binding mechanism is based on the interaction forces, which, however, are strongly modified in DM fibers; this was shown in detail in Ref. [28]. It remained open in Ref. [21] whether soliton molecules of more than two solitons exist, but there had been numerical indications [23,24,27,29].

The core of our present suggestion is that such a three-soliton molecule exists, and may be suitable for enhanced coding of data. This basic idea has already been raised in Ref. [30] where a solution of the NLSE (constant-dispersion fiber) was found that is basically a well-separated three-soliton compound. However, given the large separation of the pulses the binding forces in that situation must have been quite weak (if nonzero at all [31]). Also, two-pulse molecules in the same fiber would need to have two very unequal pulse powers which is awkward from the technical standpoint of detection at the receiver. A recent more detailed theoretical work deals with two-soliton compounds in constant-dispersion fibers [32]. While these compounds are also called soliton molecules they are qualitatively different from soliton molecules in the DM case. Also, Ref. [30] is silent about molecules containing more than two pulses. DM fibers, now the commonly deployed fiber type, are not treated in Refs. [30,32].

It must further be mentioned that soliton molecule formation has been observed inside the resonator of fiber lasers [33–42]. However, in these systems the underlying equation is not the nonlinear Schrödinger equation but the complex Ginzburg-Landau equation [42,43]; these compounds (with properties different from the ones studied here) therefore do not exist in passive fibers. Here we restrict ourselves to the nonlinear Schrödinger case because we consider it to be better compatible with actually employed real-world transmission systems.

In this paper the question of whether soliton molecules of more than two pulses exist is answered in the affirmative. We report here the experimental observation of single solitons and of two- and three-soliton molecules existing under the same circumstances in the same DM fiber. To describe all propagation effects of a pulse $u(t,z)$ in our experimental fiber line we use the following generalized dispersion-managed nonlinear Schrödinger equation:

$$\frac{\partial}{\partial z}u = i\sum_{k=2}^{K}\left\{\frac{i^k}{k!}\beta_k(z)\frac{\partial^k}{\partial t^k}u\right\} + i\gamma(z)|u|^2u - \frac{\alpha(z)}{2}u - i\gamma(z)T_{\mathrm{R}}\frac{\partial}{\partial t}|u|^2u. \quad (1)$$

Here $\beta_k(z)$ are the z-dependent dispersion parameters, and we use $K = 5$. $\gamma(z)$ is the nonlinearity parameter, $\alpha(z)$ describes the fiber and splice losses, and t is time in a comoving frame. The Raman effect is included in linearized

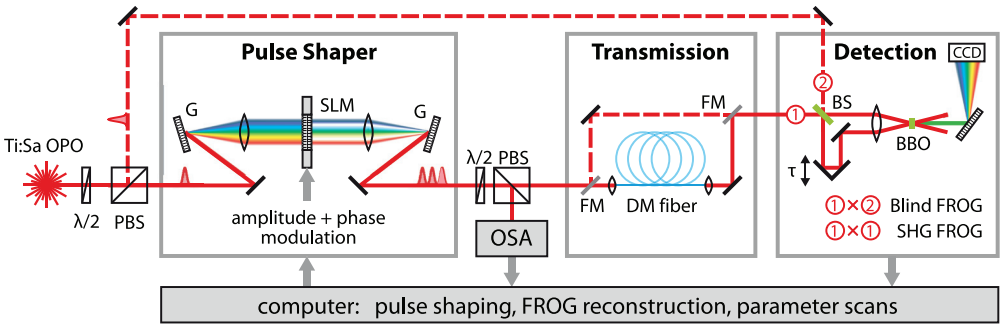

FIG. 1. (Color online) Experimental setup. The pulse shaper consists of a liquid-crystal-based spatial light modulator (SLM) with amplitude and phase masks in a $4f$ setup with two diffraction gratings (G). The desired initial shape is carved from the OPO pulses; the result is monitored by an optical spectrum analyzer (OSA). $\lambda/2$, half-wave retarder; PBS, polarizing beam splitter. The DM fiber link is described in the text. Flip mirrors (FM) steer either the fiber input or the fiber output signal towards data acquisition. BS, beam splitter; BBO, frequency-doubling β-BaB_2O_4 crystal; CCD, camera. Both second-harmonic generation (SHG) frequency-resolved optical gating (FROG) and blind FROG measurement is provided; the latter requires a sample of the OPO pulse as a reference. Both pulse shaping and data acquisition are computer controlled for automated parameter scans.

form, an approximation well justified for pulse durations of a few hundred femtoseconds; T_R is the corresponding Raman response time.

III. EXPERIMENTAL SETUP

The experimental setup for studies of soliton molecules is shown in Fig. 1. As a light source we use a commercial system consisting of a solid-state laser (Verdi V10 by Coherent, Inc.) pumping a combination of a Ti:sapphire laser and an optical parametric oscillator (OPO) (Mira by Coherent, Inc.). The output wavelength, tunable between 1480 and 1600 nm, is set to $\lambda_0 = 1540$ nm; the average output power is 200 mW. The system is mode locked and produces nearly Gaussian pulses,

$$u_{\mathrm{OPO}}(t) = \sqrt{P}\,\exp\left[-\frac{1+iC}{2}\,\frac{t^2}{T^2}\right], \tag{2}$$

where P is the peak power (typically $P = 30$ W), C is the chirp ($C \approx 0.4$), and T is the pulse duration (here, $T = 150$ fs, corresponding to a full half-width $\tau_{\mathrm{FWHM}} \approx 250$ fs). This pulse duration was required for correct scaling of the experiment (see below); it was obtained after modification of the laser system which also brought the repetition rate to $\nu_{\mathrm{rep}} = 57$ MHz. A $\lambda/2$ wave plate in combination with a polarizing beam splitter is used for power adjustments and outcoupling of a reference signal used for cross-correlation measurements (see below).

Desired pulse shapes suitable for soliton interaction measurements are carved from $u_{\mathrm{OPO}}(t)$ with a pulse-shaper setup. It consists of two gratings (G), two achromatic lenses (focal length +250 mm), and a spatial light modulator (SLM) in a symmetric $4f$ setup [44]. The SLM (CRI, Inc. model SLM-128D-NM) has two phase masks with 128-pixel resolution and allows amplitude and phase modulation in the spectral domain. In this configuration the frequency resolution is 75 GHz/pixel. This limits the shaped temporal wave forms to a duration of 13.3 ps.

As a reasonable approximation to the shape of soliton molecules we prepare a temporal complex field $u(t)$ consisting of n pairwise-antiphase Gaussian pulses with peak power P_0, pulse width T_0 (we use $T_0 = 178$ fs throughout), and separation σ_{in}. This is described by

$$u(t) = \sqrt{P_0}\,\sum_{k=1}^{n} u_k(t) \quad \text{with}$$
$$u_k(t) = \exp\left[-\frac{[2t + (n-2k+1)\sigma_{\mathrm{in}}]^2}{8T_0^2} + i\frac{(-1)^k\pi}{2}\right]. \tag{3}$$

The center of this structure is at $t = 0$ in the frame of reference of the original laser pulses. Numerical Fourier transform of Eq. (3) provides the target spectrum to be fed as control signal to the SLM (see Fig. 1). We correct this control signal according to the linear spectral chirp of the initial laser pulses. We monitor both the spectral profile of the laser pulse and the generated structure with an optical spectrum analyzer (OSA), and check the latter against the desired spectral profile. The spectral information is also used for fine-tuning of the pulse energy and for compensation of fluctuations and drift of laser power and wavelength during extensive parameter scans.

A microscope objective (20× numerical aperture 0.35 Infrared Apochromat by Nachet Vision, Dijon, France) is used to couple the pulse groups thus prepared into a custom-made DM fiber. This fiber line is a scale model of a typical commercial fiber line with 40 Gbit/s bit rate using $\tau_{\mathrm{FWHM}} = 7.5$ ps pulses. When the pulse duration τ_{FWHM} is scaled down, fiber length must be reduced accordingly in proportion to τ^2_{FWHM}. With the ≈250 fs pulses used here the dispersion period is therefore scaled down 900-fold. Our fiber link has ten dispersion periods, or 460 m of fiber, and corresponds to a real-life version with a span of just over 400 km.

Each dispersion period consists of a half segment of anomalously dispersive fiber (OFS Fitel TrueWaveSRS), a full segment of normally dispersive fiber (OFS Fitel TrueWaveRS), and another half segment of TrueWaveSRS fiber. Power losses are mostly due to the 20 splices. Each splice was assessed individually; the total loss comes to $\alpha_{\mathrm{splice}} = 1.55$ dB. We intentionally do not use amplifiers in order to preclude any possibility of influence from gain dynamics; in exchange we must accept that the pulse shapes are affected somewhat by the loss. In the scaled system pulse energy is somewhat elevated: Pulse energies of ≈10 pJ as used here correspond to ≈0.3 pJ in

TABLE I. Fiber parameters as obtained from measurement and used for numerical simulations. All dispersion values β_i are given in units of ps^i/km.

	Individual fibers		Finished DM fiber (10 periods)	
	TrueWave SRS	TrueWave RS		
L	24 m	22 m	L	460 m
β_2	-5.159	4.259	$\overline{\beta}_2$	-0.654
β_3	7.778×10^{-2}	5.948×10^{-2}	γ	1.72 W^{-1} km^{-1}
β_4	-2.524×10^{-4}	-5.636×10^{-4}	T_R	5.8 fs
β_5	7.251×10^{-14}	1.005×10^{-5}	α_{splice}	1.55 dB

a real-world system. Note that some perturbations grow faster than τ_{FWHM}^{-2}, e.g., the Raman effect as τ_{FWHM}^{-4}; this implies that in assessing complications from these effects our experiment is very conservative. All fiber parameters are listed in Table I.

Mirrors in flip mounts make it possible to switch rapidly between assessment of the shapes of either the pulses launched into the fiber link or the ones emerging from the distal end. As we are interested in obtaining both amplitude and phase information, data acquisition is centered around a homemade frequency-resolved optical gating (FROG) setup [45] which allows one to take either a second-harmonic generation (SHG) FROG spectrogram or a blind FROG spectrogram—again by flipping a beam splitter (BS). Blind FROG involves a cross correlation of the pulse under test with the reference which is taken from the otherwise unused output of the attenuator described above; note that this is a single pulse as in Eq. (2). The complex temporal and spectral field is obtained from the raw data with a standard principal components generalized projections (PCGP) pulse reconstruction algorithm [45]. For extensive parameter scans a reduced data representation was preferred, for which the SHG and blind FROG spectrograms are reduced without reconstruction to the intensity autocorrelation (IAC) or the intensity cross correlation (ICC), respectively. Both pulse shaping and data acquisition are computer controlled with LABVIEW software (National Instruments Corporation, Austin, TX, USA) for rapid data gathering in sequential runs.

The fiber length of nearly 460 m introduces a delay between the signal and reference pulses of blind FROG. One might use another delay line for the reference; however, its length would introduce stability issues. We chose to derive the reference not from the same laser pulse but from its 129th successor, so that no further delay is required. Some jitter is introduced into our measurements due to laser fluctuations on time scales from the 2μs delay to the camera exposure time of 1 s. Tests show that in comparison of IAC and ICC, the latter systematically finds the pulse duration longer by $(4.8 \pm 1.2)\%$. This error was considered a minor detriment which can be neglected. Slower fluctuations, on the time scale of 1 min, cause an apparent temporal shift of the center position of pulses which can amount up to $\approx$400 fs, but is easily removed from the data later.

Experimental tests were accompanied by full numerical simulations. We use a split-step Fourier algorithm to calculate Eq. (1). The Kerr parameter γ is obtained from pulse energy measurements and comparisons between experimental and simulated data. The dispersion parameters $\beta_{2-5}^{\pm}$ were measured using white-light interferometry. Splice losses were included as measured individually during the fiber link assembly. The Raman response time T_R was taken from fits performed on data from former experiments on Raman-shifting soliton trains [46]. The pulse-shaper setup introduces a slight spectral chirp into the launch pulses, which is also taken into account.

IV. STABILITY AND EXISTENCE REGIME OF THE TWO-SOLITON MOLECULE

In this section we present experimental evidence for the stability of the two-soliton molecule. This presentation goes beyond descriptions given earlier in Refs. [21,28,47], and serves for comparison with the description of three-soliton molecules in the next section.

Soliton pairs can be considered a stable entity ("molecule") when there is a particular equilibrium separation σ_{eq} at which interaction forces take a net zero value, and when closer pairs experience repulsion and more distant pairs attraction. To test whether this is the case we prepare pairs of Gaussian pulses in antiphase and launch them into the fiber. Data acquisition at the distal fiber end employs intensity cross-correlation measurements. As described above, an unmodified laser pulse is used as reference signal. We obtain data known as blind FROG spectrograms [45] which are easily reduced to ICC traces by integration over the frequency axis. ICC data offer direct information about the peak power ratio, the relative peak positions (expressed as their temporal separation σ), and—relevant in the three-soliton molecule case below—asymmetry of the separations. Moreover, shifts of the central frequencies of individual peaks $\Delta\omega$ can be assessed, and with the conversion

$$\frac{\partial\sigma}{\partial z} = \overline{\beta}_2 \Delta\omega = v \tag{4}$$

are translated to relative (average) velocities v; note the peculiar dimension of s m^{-1}.

Figure 2 shows measured data when input separation is varied, at three energy levels: from the left to the right column, the individual pulses have 9.8, 11.7, and 14.4 pJ, respectively. From cross correlations (top panels) the separation is extracted and shown in the left part of the lower panels. The pertaining velocity is shown adjacently in the right part. For comparison, the dashed lines repeat the initial separation (the initial velocity is zero throughout); intersections of the data with these lines indicate the absence of net change.

Note that trivially there is always an indifferent equilibrium at very large separations because interaction eventually becomes negligible. Consequently all data must tend towards the dashed lines for large initial separation. Indeed they do, but we will disregard these trivial equilibria in the following discussions. In the low-energy case there is no nontrivial equilibrium; indeed, for $\sigma_{in} > 0.9$ ps the interaction becomes negligibly weak. In the elevated-energy case one sees a collision near 0.95 ps (close distance and velocity zero), but no equilibrium. On the other hand, in the intermediate case there is an unchanged separation and simultaneously a zero velocity at $\sigma_{in} = 0.72$ ps: this is an equilibrium. More specifically, one sees that for input separations narrower than the equilibrium value the output separation is increased (i.e., there is net repulsion), whereas for wider input separations there is net attraction. Therefore this equilibrium is a stable one. The signs of the velocity above and below the equilibrium point support

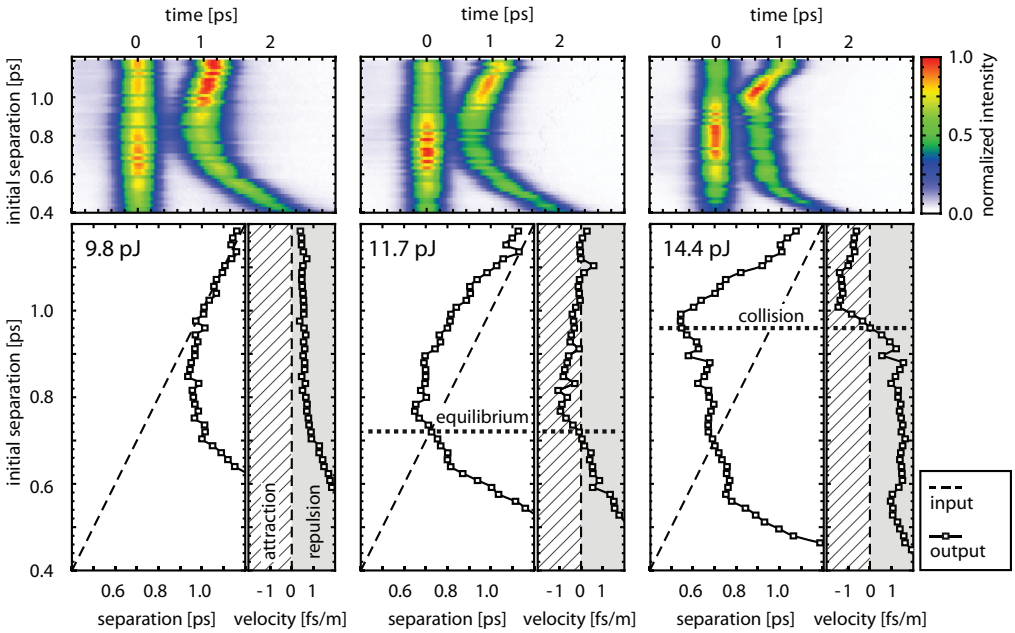

FIG. 2. (Color online) Evolution of separation between pulses in a pair when the initial separation is varied. Data are shown for three different launch energies (left, center, and right columns); the indicated numbers refer to single-pulse energies. Upper row: Cross-correlation traces measured at fiber end, color coded. The left pulse was centered on $t = 0$ to remove timing fluctuations. Lower row: Measured separation and velocity (data points) compared to initial separation (dashed lines). Stable equilibrium $\sigma_{eq} \approx 0.72$ ps is characterized by the separation crossing the input separation in the appropriate direction (see text), and simultaneously the velocity being equal to zero.

this conclusion. We have also convinced ourselves that such measured data correspond very well to simulation results [7].

A. Global parameter dependence

We proceed to map out further parameter dependencies, both close to and far away from the equilibrium position. In doing so experimentally, we have to observe one restriction. One might plot σ vs σ_{in} as a function of propagation distance along the fiber. This was done, e.g., in numerical investigations in Ref. [48] (see Fig. 4 therein). However, in an experiment it would require one to cut back the DM fiber link, destroying it in the process. It would then be impossible to repeat the investigation or test for other parameter dependencies in the same fiber. Rather than cutting back the fiber length we vary the soliton energy. Higher-energy solitons have a shorter duration and vice versa, and the overall effect is similar.

Figure 3(a) shows, at the fixed fiber length of ten dispersion periods as before, measured data of the output separation σ as a function of the initial separation σ_{in} and the pulse energy. The pulse pair energy here is twice the individual pulse energy; corrections due to destructive interference would apply for much closer separations but are minimal here. These data were obtained from 1600 individual measurements of the output-signal SHG FROG spectrograms from which the output separations are extracted. For each energy we calculated the soliton width; values $132 < T_0 < 212$ fs occurred. We then prepared the pair accordingly as two Gaussians in antiphase with the desired initial separation σ_{in}.

There are two auxiliary curves in Fig. 3(a). The dotted curve marks the equilibrium separation as predicted from calculations using an iterative averaging method. It is based on propagation simulations of the unperturbed DM NLSE [Eq. (1) with $K = 2$, $\alpha = T_R = 0$] and represents the ideal case. The long-dashed curve is similar, but from the full Eq. (1) solved numerically, and represents the realistic case. In either case the equilibrium separation decreases with increasing energy. At low energy a deviation between the two predictions is apparent. The "realistic" case requires more initial energy, with everything else the same, because it takes into account energy losses. Below ≈7 pJ there is no molecule formation at all: a threshold energy exists. Below this threshold DM solitons show only repulsion for all initial separations; they then behave similarly to fundamental solitons in constant-dispersion fibers.

In Fig. 3(b), left part, the same data set as in Fig. 3(a) are shown in a rescaled manner. The input and output separations are normalized to the numerically predicted equilibrium separation (realistic case). Therefore the equilibrium situation is now found along the horizontal dashed line. It is clearly distinguished from another regime of small output separation near the dash-dotted line: here the solitons collide right at the end of the fiber. With increasing pair energy a higher initial separation is necessary to observe a soliton collision at the fixed distance of the fiber length. Both branches split at $E_{sol} \approx 9$ pJ, just above the threshold of ≈7 pJ. The splitting point marks the lower boundary of energy where DM soliton attraction becomes dominant. The soliton molecule found at the splitting point is somewhat degenerated because there is no binding energy or restoring force.

The corresponding full numerical simulation of Eq. (1) is shown in the left part of Fig. 3(c). The two major branches are reproduced in good agreement. Differences occur in the space between: subsequent collisions can occur after the first. In each collision details of the chirp and phase affect

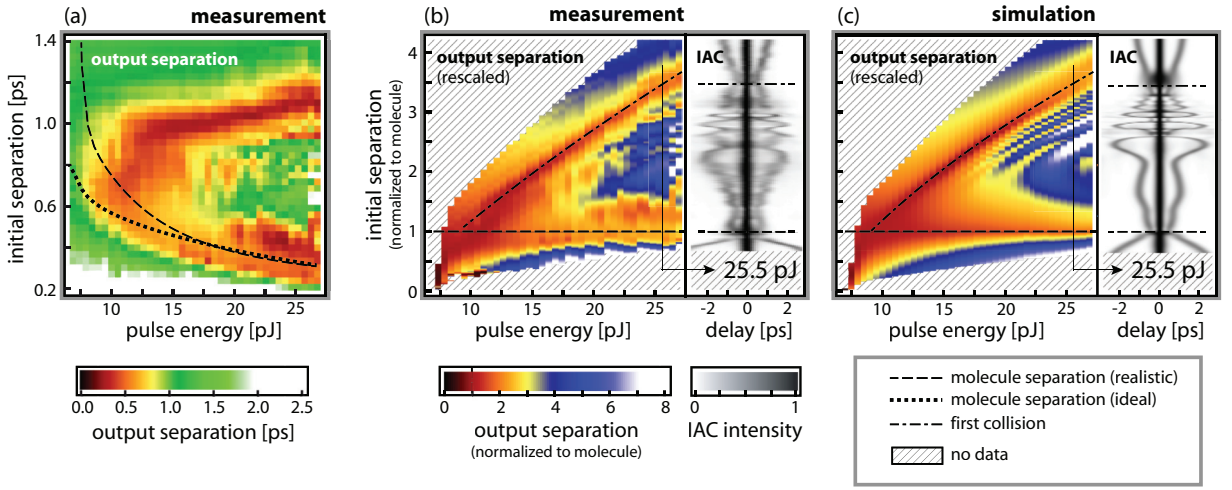

FIG. 3. (Color online) Global interaction pattern of a pair of dispersion-managed solitons. (a) Separation of DM solitons after ten dispersion periods when the pulse energy E_{sol} and initial separation σ_{in} are varied. Data are obtained from 1600 individual autocorrelation measurements. Also shown are numerically predicted equilibrium separations for the realistic (dashed line) and ideal (dotted line) cases. (b) Left side: Same data as in (a) but normalized to the respective equilibrium separation σ_{eq} of the realistic case. The branches of first collision (diagonal) and equilibrium separation (horizontal) are marked by dash-dotted and dashed lines, respectively. Right side: example of measured autocorrelation traces at $E_{\mathrm{sol}} = 25.5$ pJ in gray scale. A periodic breakup of the soliton pair is observed at $2.1\sigma_{\mathrm{eq}} < \sigma_{\mathrm{in}} < 3.1\sigma_{\mathrm{eq}}$. (c)As (b) but from full numerical simulation for comparison.

subsequent behavior, and the complex interplay may result in a self-similar (fractal) structure of the parameter space. This behavior has been studied before [48]. Both Figs. 3(b) and 3(c) are accompanied to their right by IAC traces taken at $E_{\mathrm{sol}} = 25.5$ pJ (this position is marked in the main part of the figures). The repetitive collisions are reflected in periodic changes of the output separation. Agreement is good except that the finer detail is not resolved in the experimental data.

With a view to applications of soliton molecules for data transmission, the energy region near $E_{\mathrm{sol}} \approx 11$–$16$ pJ is preferred. In this regime any complicated dynamics is absent: there is just a wide capture range for the soliton molecule.

B. Relative phase dependence

Numerical results indicate that for the stability of the two-soliton molecule their relative phase must be π. This prediction is now tested experimentally. In Fig. 4 ICC traces of fiber output signals are shown for two different single-soliton energies and for relative phases of 0 and π, respectively. For better visibility the time frame is centered on the "center of mass" of the soliton compounds. This center was determined by numerically calculating the position of maximum overlap with a broad smooth reference pulse; the necessary adjustment eliminated the timing fluctuations mentioned above. In the antiphase case the double-pulse structure is preserved for all initial separations; the repulsive regime at $\sigma_{\mathrm{in}} < 700$ fs is clearly visible. For same-phase pulses a repulsive regime is not observed; instead, pulses merge and interfere. As the center column shows, an increased energy leads to somewhat narrower equilibrium separation, but otherwise has little impact. We obtain further information about the phase dependence by continuously varying the phase difference (the phase of the leading pulse minus that of the trailing pulse) through a 2π interval at $\sigma_{\mathrm{in}} = 750$ fs (close to the equilibrium separation). This is shown in the right column. The structure is almost invariant under phase variations near both $\varphi = 0$ and $\varphi = \pi$. However, the strong dependence on σ_{in} betrays that the former lacks stability in the presence of perturbations; only the latter is quite insensitive to all parameter variations shown.

A combination of continuous phase variation and energy-level variation is given in Fig. 5. At $E_{\mathrm{sol}} = 14.4$ pJ (left panel) a deviation from $\varphi = \pi$ does not seriously disturb the two-pulse structure over our link length of ten dispersion periods. At somewhat higher energy ($E_{\mathrm{sol}} = 20.3$ pJ, center panel) the energy transfer rate due to the Raman effect is increased, but

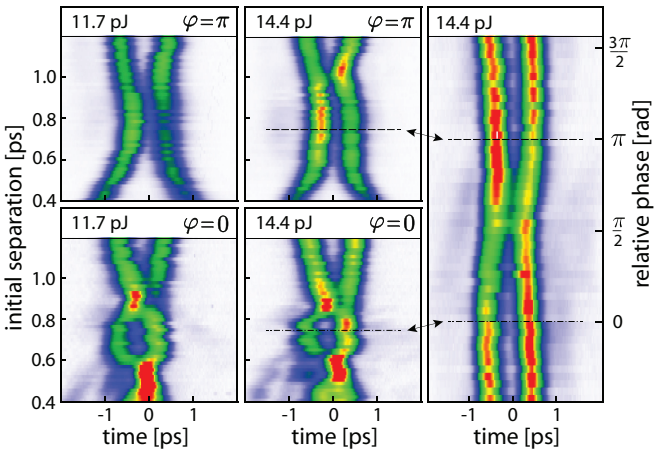

FIG. 4. (Color online) Cross-correlation measurement of fiber output signals when the parameters of the pulse pair are varied. Left column: Opposite-phase pulse pairs with 11.7 pJ pulse energy (top) and in-phase pulse pairs (bottom). Center column: Similar but at 14.4 pJ. Opposite-phase pulse pairs maintain their double-pulse structure, whereas in-phase pairs tend to merge. Right column: Continuous variation of phase difference at 14.4 pJ. Markers indicate corresponding parameters in the center column.

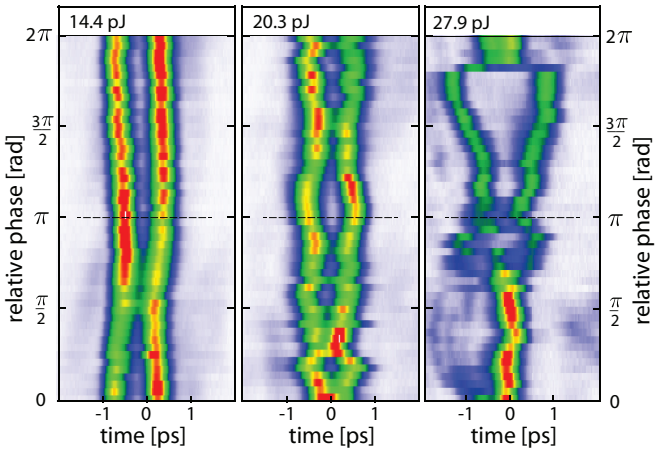

FIG. 5. (Color online) Timing of fiber output signals when the relative phase is continuously varied. Shown are ICC traces of fiber output signals at $\sigma_{in} = 750$ fs. From left to right the (single-)pulse energy is increased. At low energy the double-pulse structure remains intact at all phases; at higher values there is clear phase dependence. The pair is preserved best at the medium energy and at $\varphi = \pi$ or just above.

a two-pulse structure is still maintained. At $E_{sol} = 27.9$ pJ (right panel) there is a strong phase dependence. In a region $-\pi/4 < \varphi < 3\pi/4$ the pulses merge together; at other values they repel. As a qualitative explanation we offer the following consideration: Under the conditions here the relative phase evolves rapidly during propagation; once the pulses are in phase they mutually attract strongly and merge into a single pulse. In any event, the double-pulse structure is preserved at all energy levels shown as long as the relative phase is $\varphi = \pi$.

V. STABILITY AND EXISTENCE REGIME OF THE THREE-SOLITON MOLECULE

In this section we present an experimental demonstration of the existence of three-soliton molecules. They were predicted in Refs. [23,24,27,29] based on numerical simulations. We recently succeeded with an experimental verification, and have given a preliminary report in Ref. [7]. Here we give a full account.

Following Eq. (2), all three pulses in the triplet are prepared with the same peak power and width; they have alternating phases and are initially equidistant. We denote by σ_L the distance obtained after propagation between the leading and center pulses, and σ_T that between the trailing and center pulses. In Ref. [7] we compared autocorrelation measurements with simulations (and found close agreement). However, it takes cross correlation to do full justice to possible changes of the two separations. Figure 6 shows blind FROG data for three different pulse energy values.

The initial separations σ_{in} of the antiphase triple pulse were varied and compared with the resulting output separations σ_L and σ_T. Blind FROG traces were obtained at the fiber output; timing fluctuations described in Sec. III were removed by centering the time frames of the individual ICC traces on the maximum of the central peak. Figure 6 shows pulse separations and velocities for three different energy levels. The upper row shows the cross-correlation traces; the lower the extracted separations (left) and velocities (right). Again (compare Fig. 2), at low energy (left column) and at large separation the interaction vanishes beyond $\sigma_{in} = 0.8$ ps. At high energy collisions can occur (witness the right column at $\sigma_{in} = 0.9$ ps). However, in the intermediate case (center column) at $\sigma_{in} = 0.73$ ps there is clear indication of a stable

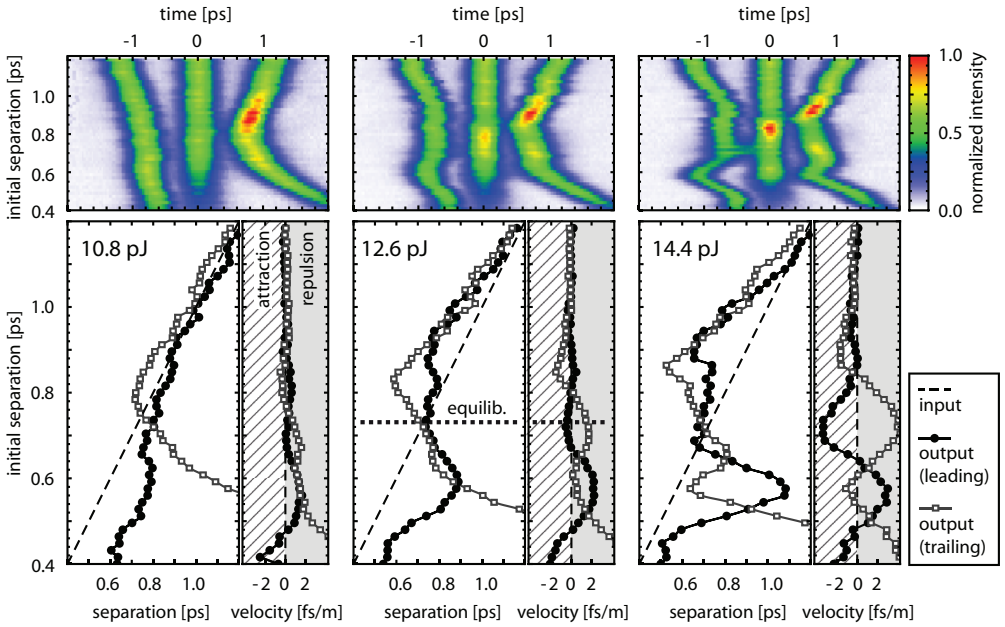

FIG. 6. (Color online) Evolution of separations between pulses in a triplet when the initial separation is varied. Data are shown for three different launch energies (left, center, and right columns); the indicated numbers refer to single-pulse energies. Upper row: Cross-correlation traces measured at the fiber end, color coded. Lower row: Measured separations and velocities. Initial separation and velocity (the latter always zero) are shown as dashed lines for comparison. See text.

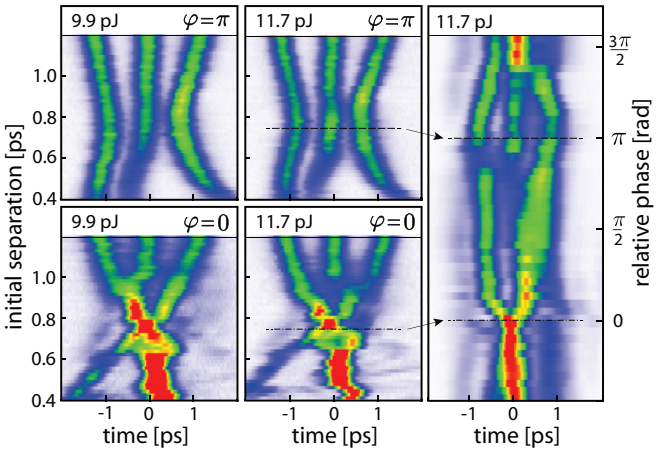

FIG. 7. (Color online) Cross-correlation measurements of fiber output signals when the parameters of the pulse triplets are varied. Left column: Soliton triplets at 9.9 pJ pulse energy with opposite (top) and same (bottom) phase. Center column: Similar but at 11.7 pJ. Opposite-phase triplets maintain their structure, whereas in-phase groups tend to collapse except for sufficiently large initial separations. Right column: Continuous variation of the phase difference at 11.7 pJ. Markers indicate corresponding parameters in the center column. The triplet structure is maintained for relative phases $0.9\pi \leqslant \varphi \leqslant 1.2\pi$; else it decays. Launch conditions: $\sigma_{\text{in}} = 750$ fs, $E_{\text{sol}} = 11.7$ pJ.

equilibrium. Only the velocity of the trailing pulse, v_{T}, has not fully died down yet, a consequence of the fact that in a realistic fiber a perfectly constant pulse shape can only be approximated. The existence of a stable equilibrium establishes the existence of three-soliton molecules.

A. Relative phase dependence

In a manner resembling that used for Fig. 4 we determined the phase dependence by comparing $\varphi = 0$ and $\varphi = \pi$; see Fig. 7. For two different energies the ICC traces of opposite-phase triple pulses are shown top left and center. The corresponding measurements for in-phase pulses are shown bottom left and center. The triple-pulse structure is maintained for $\varphi = \pi$ and all initial separations, but in the case of $\varphi = 0$ the structure collapses. Only for large initial pulse separations above $\sigma_{\text{in}} \approx 1$ ps is the structure preserved, obviously on account of the weak interaction at such large separation.

At the equilibrium separation ($E_{\text{sol}} = 11.7$ pJ, $\sigma_{\text{eq}} = 750$ fs) we continuously varied the relative phase in the range $0 \leqslant \varphi \leqslant 2\pi$; this is shown to the right. The triple-pulse shape is best maintained for relative phase values in the range $0.9\pi \leqslant \varphi \leqslant 1.2\pi$, showing that the stability and existence of the three-pulse molecules rely on a relative phase near π. Remarkably, the preferred region appears to be centered slightly above π. It is conceivable that this deviation accomplishes a certain precompensation of additional phase rotations due to higher-order dispersion and nonlinear effects.

VI. FOUR-SYMBOL TRANSMISSION

We have described so far how we combined two or three Gaussian pulses in antiphase to create the compound shapes to be launched into the fiber. We now proceed to a full amplitude and phase reconstruction of the shapes at both fiber input and output, as obtained from measured SHG FROG traces. Unfortunately SHG FROG suffers from several ambiguities, especially in the case of temporal or spectral zeros [47,49]. Therefore the field reconstructions from the measured FROG traces were repeated several times, and a low FROG error value [45], agreement between the measured and reconstructed FROG traces, and a good agreement between independently measured and reconstructed spectra were used as indicators for a correct field retrieval. Ten correct reconstructions from the same FROG trace were used to calculate the error bars shown in Fig. 8. The figure shows a single soliton (a), a two-soliton molecule (b), and a three-soliton molecule (c), respectively. Together with the absence of a pulse this set constitutes four symbols which allow quaternary coding of information. The pulse amplitude shapes obtained from numerical simulations of the generalized DM NLSE (1) are shown at the initial position (gray area) and at the fiber end (hatched area); the

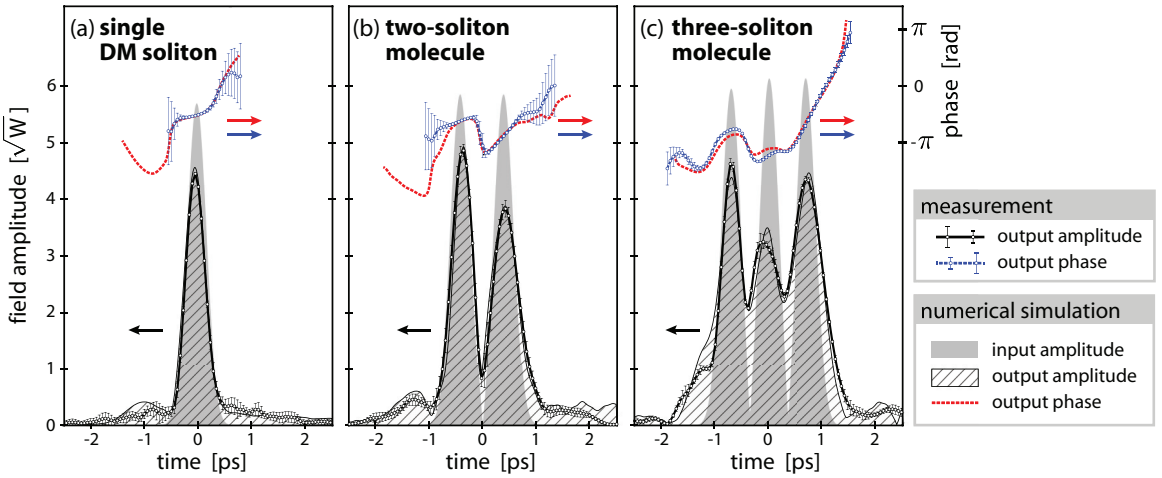

FIG. 8. (Color online) Comparison of single DM soliton (a), two-soliton molecule (b), and three-soliton molecule (c). Field amplitudes of the simulated input signals (gray area), and the same of the simulated (hatched area) and measured (black solid curve) output signals. The phase is shown in red (simulation) and blue (experimental); error bars for the latter represent scatter from repeated FROG reconstructions.

black solid line presents the experimental output shape. The corresponding phase data are shown in red (numerical) and blue (experimental).

In each case the gray and the hatched areas are the numerical input and output profiles, respectively. The power loss in the fiber is apparent; some asymmetry is introduced, and some pedestal is generated. The measured output amplitude (bold line) follows the numerical data very closely even where the shape is modified. This demonstrates that, while the shape is not perfectly maintained (as was never expected in this lossy fiber), all deviations are well accounted for. For example, the Raman effect shifts the solitons in frequency depending on their peak power so that differences in the peak powers cause slightly different frequency shifts. This corrupts the initial relative phase of π, and there is an energy transfer between the solitons. By virtue of dispersion, however, the relative phases keep evolving, and eventually this energy transfer reverses itself. In this sense the Raman perturbation is not catastrophic if unchecked: it limits its impact all by itself. Meanwhile these multisoliton compounds hang together as entities and maintain their equilibrium separation.

Note that for technical application, a FROG measurement is certainly not required; straightforward energy detection with thresholding is sufficient. For the data of Fig. 8 the symbol energies were measured as 10.5, 22.2, and 35.1 pJ, respectively; this corresponds to a ratio of 1:2.1:3.3, which is fairly close to the ideal integer 1:2:3 relation.

VII. CONCLUSIONS

In conclusion we have experimentally investigated interactions of adjacent dispersion-managed solitons and could demonstrate stable equilibrium positions of neighboring pulses. In this way we could demonstrate the existence and determine regimes of stability for soliton molecules involving two or three solitons. There is a range of pulse energies for which the soliton molecules maintain their structure best. Below that energy range the interaction is too weak to form a stable equilibrium; at higher energies higher-order effects become detrimental. Transmission without errors will not be possible over unlimited distances, but for realistic long-haul transmission lines soliton molecules appear feasible.

Our setup was designed to produce experimental evidence, i.e., a proof of principle, that a molecule of three solitons exists. It was supposed to provide detailed information about pulse shapes and small perturbations thereof, in order to help detailed understanding. It was not designed, nor is it suitable, for actual transmission tests. The setup is limited in speed not only by the time needed for data acquisition using a FROG algorithm; it is also limited by the time it takes to set the pulse shaper to parameters suitable for the next symbol. Both these times are on the order of 1 s.

Of course, a system designed for technical application would not be restricted by these factors. All symbols would be generated simultaneously by a combination of several diode lasers and some micro-optic circuitry, and the desired symbol would be routed to the fiber by electro-optic modulators fast enough to respond within the clock period. Such modulators are commercially available for data rates up to 100 Gbits/s. At the receiver end, it will suffice to determine the energy of each symbol. This can be done adequately by fast photodiodes combined with three threshold detectors; such technology also exists.

Once such tests are made it will also be critically important to study intersymbol interactions because any application will involve wavelength division multiplexing. Such studies for ordinary and dispersion-managed solitons showed that degradation of data integrity due to collisions is manageable [11]; a similar assessment for soliton molecules has not been performed yet.

Finally we point out that the use of different soliton molecules advocated here does in no way interfere with the use of different states of polarization, or different phases. It should be noted that all four symbols described here have a well-defined state of polarization (constant linear) and phase (there are two opposite values even when the chirp evolves in the dispersion period). Therefore, coding based on soliton molecules can be combined with both polarization and phase multiplexing schemes. One may anticipate that the latter schemes will benefit from the soliton molecule concept by a twofold increase of their data rate.

ACKNOWLEDGMENT

Financial support by Deutsche Forschungsgemeinschaft is gratefully acknowledged.

[1] C. E. Shannon, Bell Syst. Tech. J. **27**, 379 (1948).
[2] J. M. Kahn and K.-P. Ho, Nature (London) **411**, 1007 (2001).
[3] P. P. Mitra and J. B. Stark, Nature (London) **411**, 1027 (2001).
[4] K. S. Turitsyn and S. K. Turitsyn, Opt. Lett. **37**, 3600 (2012).
[5] D. J. Richardson, Science **330**, 327 (2010).
[6] G. Li, Adv. Opt. Photonics **1**, 279 (2009).
[7] P. Rohrmann, A. Hause, and F. Mitschke, Sci. Rep. **2**, 866 (2012).
[8] A. Hasegawa and F. Tappert, Appl. Phys. Lett. **23**, 142 (1973).
[9] L. F. Mollenauer, R. H. Stolen, and J. P. Gordon, Phys. Rev. Lett. **45**, 1095 (1980).
[10] G. Agrawal, *Nonlinear Fiber Optics*, 4th ed. (Academic Press, San Diego, 2007).
[11] L. F. Mollenauer and J. P. Gordon, *Solitons in Optical Fibers: Fundamentals and Applications* (Academic Press, San Diego, 2006).
[12] J. H. B. Nijhof, N. J. Doran, W. Forysiak, and F. M. Knox, Electron. Lett. **33**, 1726 (1997).
[13] Y. Chen and H. A. Haus, Opt. Lett. **23**, 1013 (1998).
[14] S. K. Turytsin and E. G. Shapiro, Opt. Lett. **23**, 682 (1998).
[15] J. N. Kutz and S. G. Evangelides, Opt. Lett. **23**, 685 (1998).
[16] V. S. Grigoryan and C. R. Menyuk, Opt. Lett. **23**, 609 (1998).
[17] N. J. Smith, F. M. Knox, N. J. Doran, K. J. Blow, and I. Bennion, Electron. Lett. **32**, 54 (1996).
[18] S. Turitsyn, E. Shapiro, S. Medvedev, M. P. Fedoruk, and V. Mezentsev, C. R. Phys. **4**, 145 (2003).

[19] J. P. Gordon, Opt. Lett. **8**, 596 (1983).
[20] F. Mitschke and L. F. Mollenauer, Opt. Lett. **12**, 355 (1987).
[21] M. Stratmann, T. Pagel, and F. Mitschke, Phys. Rev. Lett. **95**, 143902 (2005).
[22] C. Paré and P.-A. Bélanger, Opt. Commun. **168**, 103 (1999).
[23] A. Maruta, T. Inoue, Y. Nonaka, and Y. Yoshika, IEEE J. Sel. Top. Quantum Electron. **8**, 640 (2002).
[24] M. J. Ablowitz, T. Hirooka, and T. Inoue, J. Opt. Soc. Am. B **19**, 2876 (2002).
[25] B.-F. Feng and B. A. Malomed, Opt. Commun. **229**, 173 (2004).
[26] S. Johnson, S. Pau, and F. Küppers, J. Lightwave Technol. **29**, 3493 (2011).
[27] F. J. Diaz-Otero and P. Chamorro-Posada, Opt. Commun. **285**, 162 (2012).
[28] A. Hause, H. Hartwig, M. Böhm, and F. Mitschke, Phys. Rev. A **78**, 063817 (2008).
[29] A. Maruta and Y. Yoshika, Eur. Phys. J.: Spec. Top. **173**, 139 (2009).
[30] N. N. Akhmediev, G. Town, and S. Wabnitz, Opt. Commun. **104**, 385 (1994).
[31] B. A. Malomed, Phys. Rev. A **44**, 6954 (1991).
[32] U. Al Khawaja, Phys. Rev. E **81**, 056603 (2010).
[33] Ph. Grelu, F. Belhache, F. Gutty, and J. M. Soto-Crespo, J. Opt. Soc. Am. B **20**, 863 (2003).
[34] D. Y. Tang, B. Zhao, D. Y. Shen, C. Lu, W. S. Man, and H. Y. Tam, Phys. Rev. A **68**, 013816 (2003).
[35] D. Y. Tang, L. M. Zhao, and B. Zhao, Appl. Phys. B: Lasers Opt. **80**, 239 (2005).
[36] B. Ortaç, A. Zaviyalov, C. K. Nielsen, O. Egorov, R. Iliew, J. Limpert, F. Lederer, and A. Tünnermann, Opt. Lett. **35**, 1578 (2010).
[37] V. V. Afanasjev and N. Akhmediev, Opt. Lett. **20**, 1970 (1995).
[38] Ph. Grelu, M. Grapinet, J. M. Soto-Crespo, and N. Akhmediev, PIERS Online **3**, 357 (2007).
[39] A. Zavyalov, R. Iliew, O. Egorov, and F. Lederer, Phys. Rev. A **80**, 043829 (2009).
[40] A. Chong, W. H. Renninger, and F. Wise, Opt. Lett. **33**, 1717 (2008).
[41] N. D. Nguyen and L. N. Binh, Opt. Commun. **281**, 2012 (2008).
[42] Ph. Grelu and N. Akhmediev, Nat. Photonics **6**, 84 (2012).
[43] N. N. Akhmediev, A. Ankiewicz, and J. M. Soto-Crespo, Phys. Rev. Lett. **79**, 4047 (1997).
[44] A. M. Weiner, Rev. Scient. Instrum. **71**, 1929 (2000).
[45] R. Trebino, *Frequency Resolved Optical Gating: The Measurement of Ultrashort Laser Pulses* (Kluwer Academic, Boston, 2002).
[46] A. Hause, P. Rohrmann, H. Hartwig, and F. Mitschke, in *Proceedings of the Quantum Electronics and Laser Science Conference*, OSA Technical Digest (Optical Society of America, Washington, DC, 2011), paper JThB56.
[47] A. Hause, H. Hartwig, B. Seifert, H. Stolz, M. Böhm, and F. Mitschke, Phys. Rev. A **75**, 063836 (2007).
[48] A. Hause, H. Hartwig, and F. Mitschke, Phys. Rev. A **82**, 053833 (2010).
[49] D. Keusters, H-S. Tan, P. O'Shea, E. Zeek, R. Trebino, and W. S. Warren, J. Opt. Soc. Am. B **20**, 2226 (2003).